Figure 7. As in Fig. 4 but for the southwest monsoon season (July to October). Panel **(t)** displays the location of the monthly 29-year area-weighted average precipitation rate in Fig. 9 as a black dashed box (85–90° E, 20–25° N).

low h_2. In June and October, coastal regions have the highest radiant heating rate difference between the control and perturbation runs (Fig. 10a, b). In June, the area-weighted mean radiant heating rate in the coastal region of the Irrawaddy Delta increases by 0.4 °C per month in the perturbation run (Fig. 10a). A h_2 decrease of 9 m has the largest contribution to the radiant heating rate increase of 0.7 °C per month (Fig. 11a) compared with an MLD decrease of 0.2 m (Fig. 10e), which contributes to less than 0.1 °C per month (Fig. 11e). A decrease in the downward shortwave radiation flux of 8 W m^{-2} (Fig. 10c), associated with an increase in monsoon cloud cover, cools the region by 0.3 °C per month

(Fig. 11c). In October, the radiant heating rate difference in the Irrawaddy Delta increases by 1.5 °C per month in the perturbation run (Fig. 10b). The radiant heating rate difference is larger than June because of an increase in the monthly average downward shortwave radiation flux and a shallower MLD in both the control and perturbation runs. A decrease in h_2 of 9 m has the largest contribution to the radiant heating rate increase of 1.4 °C per month (Fig. 11a), whereas a decrease in the MLD of 0.1 m (Fig. 10f) and an increase in downward shortwave radiation flux of 1 W m^{-2} (Fig. 10d) only contribute to less than 0.1 °C per month of the increase in radiant heating rate respectively (Fig. 11d, f). The changes
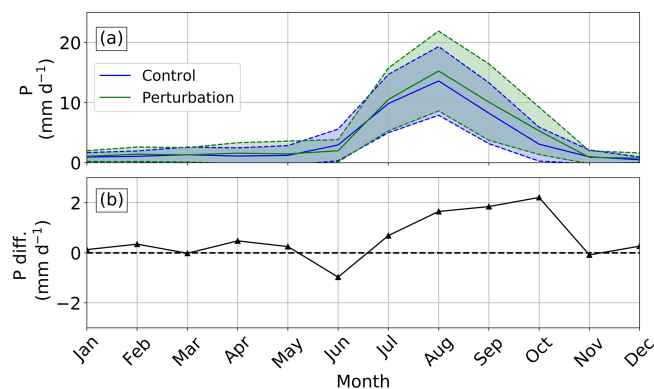
Figure 8. (a) Monthly 29-year area-weighted average precipitation rate for the control run (blue solid line) and the perturbation run (green solid line) for the 85–90° E, 20–25° N region. The shaded region between the dashed lines shows the 1 standard deviation variability. **(b)** The difference in the monthly 29-year area-weighted average precipitation rate between the control and perturbation run.

in h_2 are more influential on the mixed layer radiant heating rates and SSTs compared with small changes in MLD and downward shortwave radiation flux in the Irrawaddy Delta during June and October.

In June, the area-weighted mean radiant heating rate difference in the SMC region decreases by 0.1°C per month in the perturbation run (Fig. 10a). A decrease in the downward shortwave radiation flux of $5\,\mathrm{W\,m^{-2}}$ (Fig. 10c) has the largest contribution to the radiant heating rate decrease of 0.1 °C per month (Fig. 11c), whereas a decrease in h_2 of 2 m and an increase in MLD of 0.4 m (Fig. 10e) contribute less than 0.1 °C per month to the radiant heating rate (Fig. 11a, e). In October, the radiant heating rate difference of the SMC region shows an increase of 0.1 °C per month (Fig. 10b). A decrease in h_2 of 3 m has the largest contribution to the radiant heating rate increase of 0.1 °C per month (Fig. 11b), whereas a decrease in the downward shortwave radiation flux of $1\,\mathrm{W\,m^{-2}}$ (Fig. 10d) and an increase in MLD of 0.2 m (Fig. 10f) contribute less than 0.1 °C per month to the radiant heating rate (Fig. 11d, f). In the SMC region, changes in h_2 are smaller than those in coastal regions during June and October. Thus, changes in h_2 and indirect changes in MLD and downward shortwave radiation exert a comparable control on the open-ocean mixed layer radiant heating rate and SST.

The radiant heating rate of the mixed layer and the resultant change in the SST further depend on the seasonal changes in the depth of the mixed layer relative to the solar penetration depth (Turner et al., 2012). Here, we examine how the depth of the mixed layer relative to the solar penetration depth affects mixed layer radiant heating rates and SSTs for the open-ocean region of the SMC and the coastal region of the Irrawaddy Delta during June and October.

In the Irrawaddy Delta region during October, the MLD shoals to 9 m (green dashed line in Fig. 12b), which is similar

to the perturbed h_2 (green dot in Fig. 12b). When the mixed layer is shallow, the increased near-surface radiant heating from reducing h_2 is distributed to a shallower depth, increasing the average change in the radiant heating rate by 1.2°C per month ($\Delta \mathrm{d}T/\mathrm{d}t$; Fig. 12f). Below a depth of 10 m, radiant heating rates decrease due to reduced h_2. There is also no change in the MLD in response to reduced h_2 in the perturbation run. The increase of $0.8\,\mathrm{m\,s^{-1}}$ in the local wind speed is likely to have de-stratifying effects on the upper ocean that oppose the stratifying effects of increased mixed layer radiant heating. When the MLD deepens below 10 m, the biologically induced effects of the increased radiant heating rates above 10 m and the decreased radiant heating rates below 10 m are mixed, reducing the net effect of biological heating on the mixed layer temperature. In June, the MLD deepens to 16 m (Fig. 12a), resulting in a smaller average radiant heating rate change of 0.4 °C per month (Fig. 12e). Consequently, the October SST increases by 0.5 °C compared with the smaller increase of 0.2 °C in June. Hence, shoaling the mixed layer to a depth comparable to the perturbed solar penetration depth in October limits the turbulent mixing processes to a depth where chlorophyll perturbs solar radiation absorption and makes the SST more sensitive to chlorophyll concentration changes.

In the SMC region during October, the MLD shoals to 28 m (Fig. 12d), approximately twice the depth of the perturbed h_2, resulting in an average change in the mixed layer radiant heating rate of 0.1 °C per month (Fig. 12h). As in the Irrawaddy Delta region, there is no change in the MLD in response to biological warming in the SMC region due to the $0.8\,\mathrm{m\,s^{-1}}$ increase in the local wind speed, which is likely to oppose the stratifying effects of increased mixed layer radiant heating. During June, the MLD extends to 36 m (Fig. 12c), resulting in an average change in the mixed layer radiant heating rate of less than 0.1 °C per month (Fig. 12g). As in the Irrawaddy Delta region, the effect of chlorophyll on upper-ocean temperature depends on the MLD in the SMC region, with the shallowest MLD and largest change in radiant heating rate in October. With lower chlorophyll concentrations in the SMC region than the Irrawaddy Delta region, the resultant change in SMC regional average radiant heating rate in the top 10 m is considerably lower.

4 Discussion and conclusions

In this study, we have identified that the influence of biological warming on the South Asian monsoon strongly depends upon the seasonality of the chlorophyll concentration and the depth of the mixed layer, which is further dependent on the timing of the monsoon itself. The effect of chlorophyll on the SST is amplified during the inter-monsoon periods when shallow MLDs are comparable to the perturbed solar penetration depths. The MLD and its effect on the biological warming vary seasonally and spatially in the BoB. Coastal
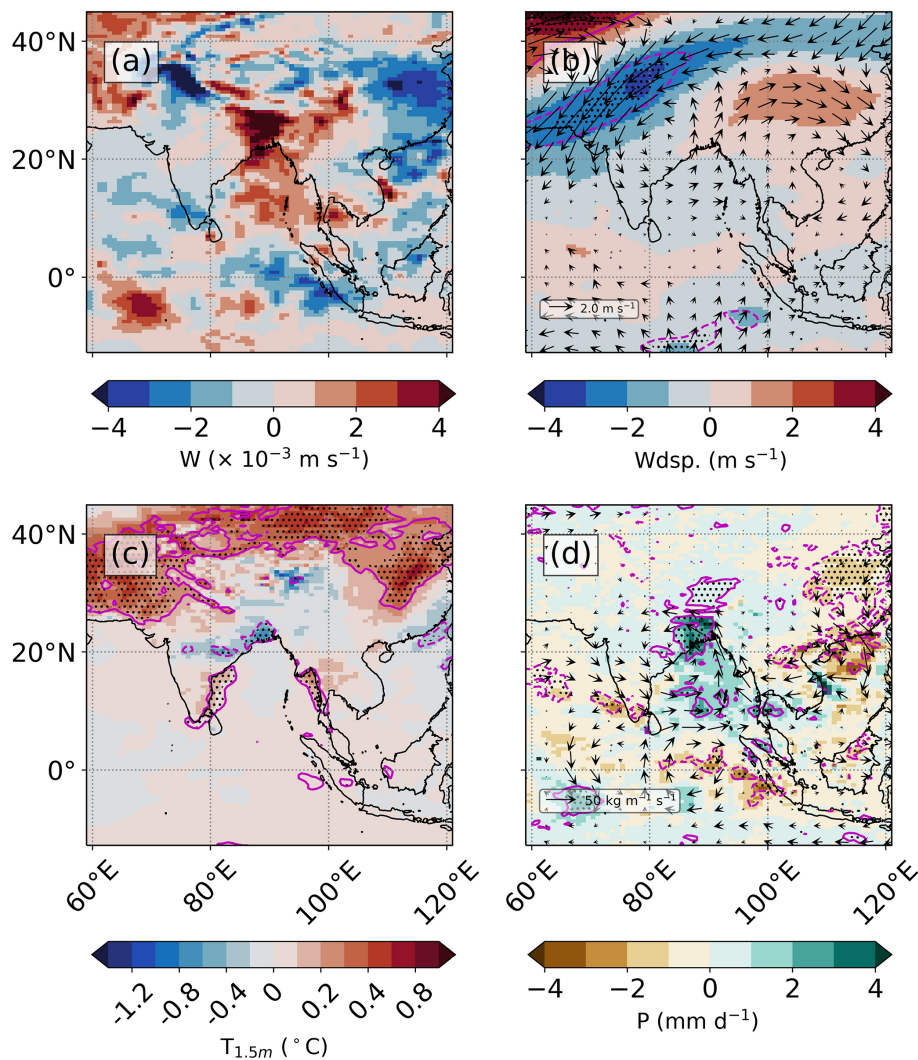
Figure 9. October 29-year average difference (perturbation minus control) of **(a)** the 500 hPa vertical velocity (m s^{-1}), **(b)** the 200 hPa horizontal vector wind (m s^{-1}), **(c)** the 1.5 m air temperature (°C), and **(d)** the precipitation rate (mm d^{-1}) and VIMF (kg m^{-1} s^{-1}). The magenta line shows the 10 % significance level, and the black stippling shows the 5 % significance level.

regions experience larger SST increases than open-ocean regions due to higher chlorophyll concentrations and shallower MLDs. The SST increase is larger during the autumn inter-monsoon (September–October) than during the spring inter-monsoon (April–May) and southwest monsoon onset (June). During the spring inter-monsoon, chlorophyll concentrations are low across the open ocean, but they remain high in coastal regions. During the southwest monsoon onset, chlorophyll concentrations are high when the MLD is relatively shallow (< 30 m) in the northern and western coastal BoB, leading to an increased SST. During the autumn inter-monsoon, high chlorophyll concentrations extend over the continental shelf in the northern BoB, the SMC region, and the eastern BoB, which is in contrast to the spring inter-monsoon when high chlorophyll concentrations are confined to the coasts. The chlorophyll concentrations in the southwestern and north-

western BoB peak in August and October respectively (Lévy et al., 2007), whilst the MLD is shallowest across the basin, which results in an increase in the mixed layer radiant heating rate and SST in the western BoB in autumn.

The direct changes in h_2 in coastal regions are large and, thus, more influential on the mixed layer radiant heating rate and SST. The resultant increase in the radiant heating rate of the coastal mixed layer and SST during the southwest monsoon onset and autumn inter-monsoon increases the latent heat flux and the transport of moisture to the Indian subcontinent. Precipitation rates over the Myanmar coast during the southwest monsoon onset increase by 3 mm d^{-1}. Comparing the monthly average precipitation rate difference (Fig. 4o) with the control simulation bias (Fig. 13a) shows that the model dry bias of 4 mm d^{-1} over the Myanmar coast is partly removed in the perturbation run. Precipitation rates
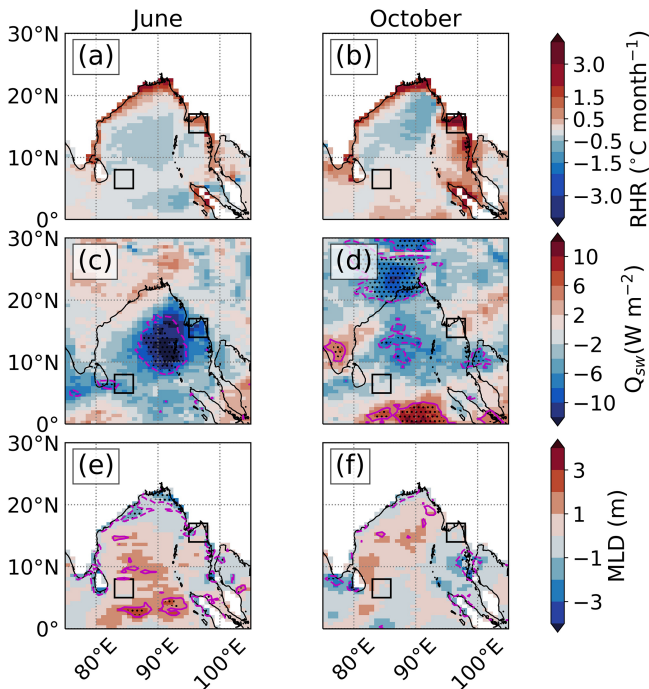
Figure 10. Monthly 29-year average difference (perturbation minus control) of **(a, b)** the radiant heating rate (°C per month), **(c, d)** the downward shortwave radiation flux (W m^{-2}), and **(e, f)** the mixed layer depth (m) for June and October. The black boxes show the location of the open-ocean region of the SMC (southwestern BoB; 83–86° E, 5–8° N) and the coastal region of the Irrawaddy Delta (northeastern BoB; 95–98° E, 14–17° N). The magenta line shows the 10 % significance level, and the black stippling shows the 5 % significance level.

over western Bangladesh and northeastern India during the autumn inter-monsoon increase by 3 mm d^{-1}. Comparing the precipitation differences (Fig. 7t) with the model bias (Fig. 13b) shows that the model dry bias of up to 3 mm d^{-1} over northeastern India is removed in the perturbation run. The reduced model biases after imposing a more accurate representation of chlorophyll further highlights the importance of including chlorophyll in coupled models.

Figure 14 illustrates and summarizes the effect of chlorophyll during the summer monsoon onset in the BoB interior where mixed layers are shallow (30 m) and where there is a zonal gradient in the mixed layer turbidity. Chlorophyll concentrations are high (1 mg m^{-3}) and values of h_2 are low (8 m) to the west, and chlorophyll concentrations are low (0.1 mg m^{-3}) and values of h_2 are high (20 m) to the east. The mixed layer radiant heating rates would increase (ΔRHR > 0) in the high chlorophyll concentration region, which reduces the radiant heating rates (ΔRHR < 0) below the mixed layer. Increasing the mixed layer radiant heating rate increases the mixed layer temperature and SST (ΔSST > 0). The upward latent heat flux and evaporation increases with increasing SST and strengthening monsoon
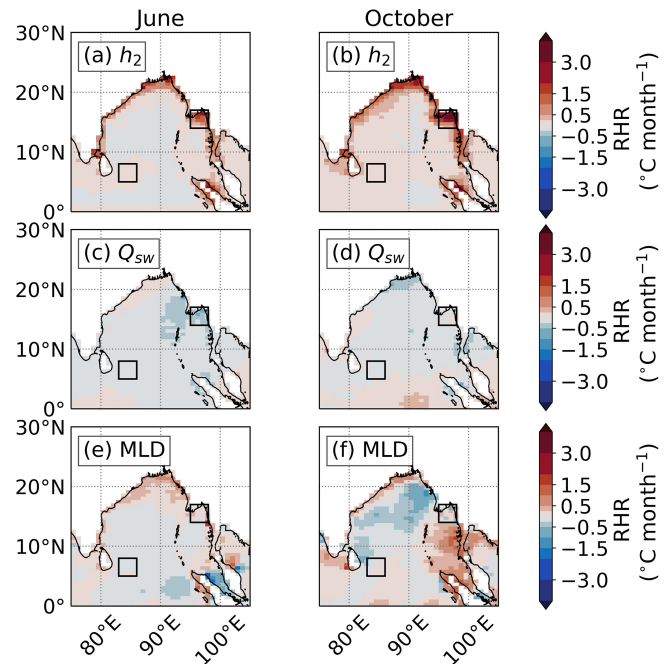
Figure 11. Monthly 29-year average difference (perturbation minus control) of the estimated relative contribution to changes in the radiant heating rate (°C month^{-1}) from **(a, b)** h_2, **(c, d)** the downward shortwave radiation flux, and **(e, f)** the MLD for June and October. As in Fig. 10, the black boxes show the location of the open-ocean SMC region and the coastal Irrawaddy Delta region.

winds. Convergence of the additional lower-tropospheric moisture that is transported by the monsoon winds increases the precipitation rates to the east.

During October, the enhanced precipitation rate and convective activity in the northern BoB perturbs upper-tropospheric winds, potentially causing reduced precipitation rates over eastern China, similar to the Silk Road effect. The Silk Road pattern has been found to influence extreme heat waves over eastern China, causing considerable socio-economic devastation (Thompson et al., 2019). Indeed, the model displays significantly warmer surface temperatures in this region at this time (Fig. 9c). The Silk Road pattern dynamics have been previously linked to the South Asian summer monsoon (Stephan et al., 2019). Diverging upper-tropospheric winds caused by precipitation anomalies over the Indian subcontinent interact with midlatitude westerlies, which influences the strength and positioning of the subtropical northwestern Pacific anticyclone over eastern China (Ding and Wang, 2005; Hu et al., 2012a). The effect of chlorophyll on the midlatitude Rossby wave train and its potential impact on the East Asian climate needs further investigation.

Turner et al. (2012) identified a similar modulation of the seasonal SST cycle by the MLD after imposing seasonally varying chlorophyll concentrations in the Arabian Sea. During the spring inter-monsoon, a peak in surface chlorophyll
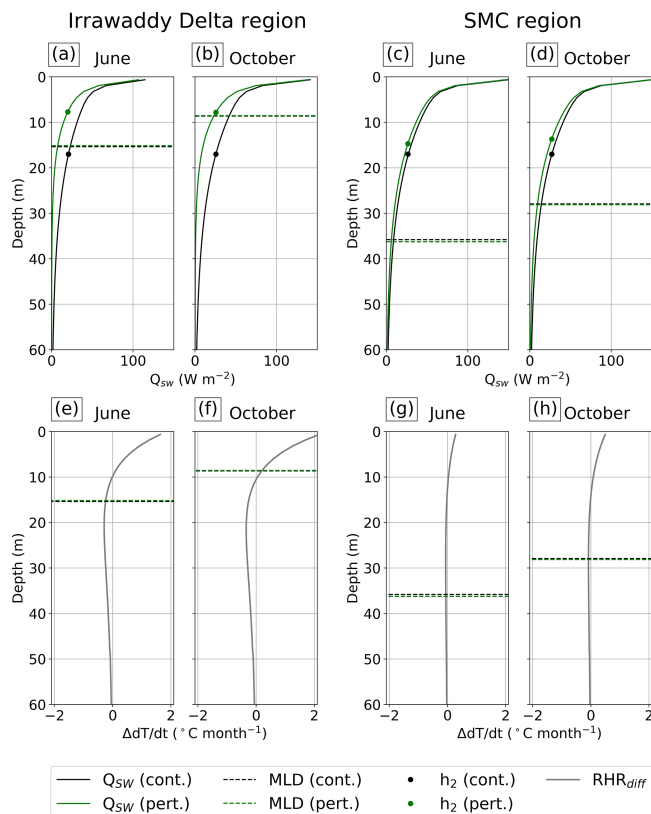
Figure 12. Panels **(a)** to **(d)** show vertical profiles of the downward shortwave radiation flux from 0 to 60 m for the control (black) and perturbation (green) run for the Irrawaddy Delta region and the SMC region during **(a, c)** June and **(b, d)** October. Panels **(e)** to **(h)** show vertical profiles of the radiant heating rate difference from 0 to 60 m during **(e, g)** June and **(f, h)** October. Dashed lines show the area-weighted 29-year average mixed layer depth, and coloured dots show the area-weighted average scale depth.
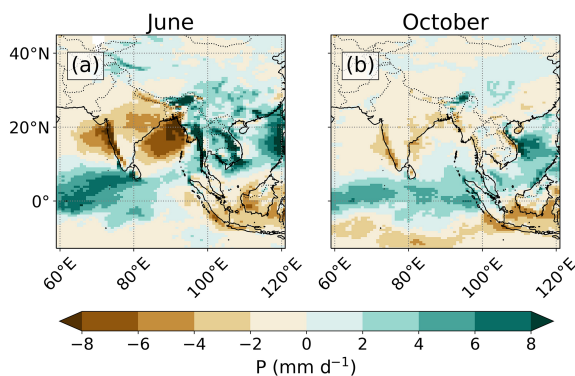

Figure 13. Model bias of the precipitation rate for **(a)** June and **(b)** October. Bias calculated as the monthly 29-year average precipitation rate from the control run minus the monthly climatological precipitation rate observed from the TRMM satellite.

concentrations and shallow MLDs led to an increase in the SST. During the autumn inter-monsoon, another peak in the surface chlorophyll concentration led to a similar but weaker increase in the SST due to deeper MLDs and stronger turbulent surface fluxes. The BoB has less biological productivity than the Arabian Sea due to light and nutrient limitation (Kumar et al., 2002), although chlorophyll concentrations in the coastal BoB can be as high as in the Arabian Sea. The BoB is also exposed to the same monsoonal winds as the Arabian Sea. Such localized, physical forcing modulates the MLD, which, in turn, modulates the biological warming. Hence, the SST increase of 0.5 °C in coastal regions of the BoB during the spring and autumn inter-monsoons is similar to the increase in the SST in the Arabian Sea during the spring inter-monsoon.

Previous studies show that the effect of biological warming is amplified due to secondary feedbacks on the MLD. In the Arabian Sea, high chlorophyll concentrations increase solar radiation absorption and, in turn, thermal stratification, which inhibits vertical mixing, shoals the MLD, and further increases the SST (Nakamoto et al., 2000; Wetzel et al., 2006; Turner et al., 2012). In our study, secondary feedbacks on the MLD are consistent in magnitude with the Arabian Sea studies. The maximum MLD difference is 3 m in the central BoB in June. Coastal MLDs shoaled around the southernmost tip of India and the northern BoB in June by $\sim$ 1 m, and the MLDs shoaled around the Kra Isthmus in October by $\sim$ 1 m (Fig. 10e, f). The effect of high chlorophyll concentrations in these localized coastal regions appears to have altered upper-ocean thermal stratification when there was little or no change in wind speed, whereas changes in wind speed primarily alter upper-ocean thermal stratification over the majority of the BoB.

In our study, a realistic chlorophyll distribution increased the open-ocean SST by $\sim$ 0.1 °C and increased the coastal SST by $\sim$ 0.5 °C during the inter-monsoons and southwest monsoon onset. The simulated increase in the open-ocean SST is consistent with previous work (Murtugudde et al., 2002; Wetzel et al., 2006). However, the increase in the coastal SST, primarily in the eastern BoB coastal region, is larger in magnitude than that reported in previous work: Wetzel et al. (2006) underestimated seasonal chlorophyll concentrations in the BoB coastal regions, while Murtugudde et al. (2002) used a low-resolution annual mean chlorophyll concentration which removed the seasonal variability of chlorophyll concentration. In this study, we impose an annual cycle of daily h_2 across the BoB; hence, the coastal and open-ocean SST responses are more accurately represented here than in previous work.

The derivation of the imposed annual cycle of h_2 in coastal regions has limitations. Firstly, the ocean colour algorithms used to determine chlorophyll concentrations from satellite are not completely effective in turbid coastal waters (Morel et al., 2007; Tilstone et al., 2013). Organic and inorganic constituents such as coloured dissolved organic matter (CDOM)
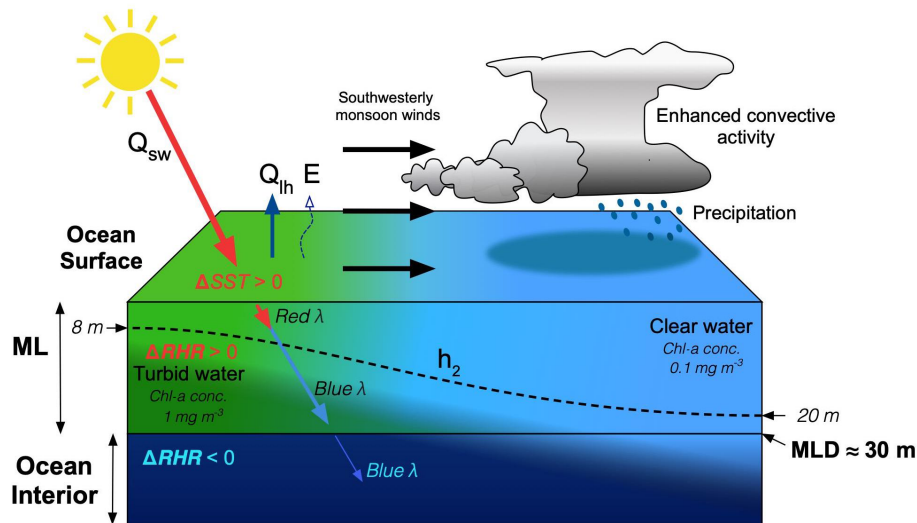
Figure 14. Schematic of the effect of chlorophyll-induced heating on monsoon rainfall in the interior of the BoB. The high chlorophyll concentration in the mixed layer (ML) affects the penetration of the shortwave radiative heat flux (Q_{sw}), the scale depth of blue light (h_2), and the difference in mixed layer radiant heating rate (ΔRHR) and SST (ΔSST) relative to clear water, which further affects the surface latent heat flux (Q_{lh}) and evaporation (E). The thick red and blue arrows pointing downwards in the mixed layer illustrate the preferential absorption of the shallow penetrating red light and the deep penetrating blue light respectively. The thin blue arrow pointing downwards below the mixed layer shows the small fraction of penetrative blue light below the mixed layer. The dashed black line in the mixed layer represents h_2. The three solid black arrows across the ocean surface represent the southwesterly monsoon winds transporting heat and moisture that sustain enhanced convection and precipitation over the interior of the BoB.

and suspended sediments strongly attenuate blue light and are, thus, falsely identified as a chlorophyll-a pigment, which typically leads to an overestimation in chlorophyll concentration (Morel et al., 2007). Secondly, the Morel and Antione (1994) chlorophyll parameterization is not applicable for coastal waters, as the parameterization is based on absorption by chlorophyll-a pigments and not by the attenuation of other in-water constituents. Missing h_2 values in the Ganges River delta are interpolated from neighbouring h_2 values that are likely associated with a satellite product and parameterization uncertainty. The Ganges coastal region has been found to influence the spring inter-monsoon SST and precipitation rates in the northern BoB. Possible positive biases in the chlorophyll concentration in the Ganges River delta are likely to lead to an overestimation of the coastal biological warming, SST, and precipitation rate increase. Ocean colour algorithms to determine proxy coastal chlorophyll concentrations are still an area of active research (Blondeau-Patissier et al., 2014). Future studies should consider the attenuation of solar radiation from other oceanic constituents in turbid coastal regions to better represent radiant heating in the upper ocean.

CDOM is a common oceanic constituent that perturbs solar penetration depths. The derived values of h_2 incorporate the bio-optical property of the chlorophyll-a pigment concentration, largely excluding CDOM. CDOM increases the radiant heating rate of nearshore coastal waters of North America (Chang and Dickey, 2004) and the Arctic (Hill,

2008). Imposing an annual mean of remotely sensed CDOM absorption coefficients in a coupled ocean–atmosphere GCM reduced solar penetration depths and increased the coastal SST in the Northern Hemisphere during the summer (Kim et al., 2018). CDOM concentrations are high in the western and northern coastal regions of the BoB at the mouths of major rivers (Pandi et al., 2014). Thus, including the bio-optical properties of CDOM and other biological constituents would likely increase the coastal SST in the BoB, with additional implications for regional climate.

The chlorophyll concentration in the BoB upper ocean is not homogeneous with depth. In situ observations show that the vertical depth of chlorophyll maxima varies between 10 and 80 m (Thushara et al., 2019; Pramanik et al., 2020), often occurring at depths undetected by satellite radiometer sensors (Huisman et al., 2006). Variations in the vertical depth of the chlorophyll maxima would vary the vertical depth of enhanced radiant heating. However, if the depth of the chlorophyll maxima occurs at a depth where solar radiation is significantly reduced (e.g. at the euphotic depth where solar radiation is $\sim 1\%$ of its surface value), the change in the local radiant heating at that depth would be negligible (Morel and Antione, 1994). Indeed, observations show the occurrence of intense deep chlorophyll maxima in the BoB at depths from 20 to 40 m (Thushara et al., 2019), which might have a strong influence on local mixed layer radiant heating and vertical heat distributions. Hence, the effect of nonuniform chloro-

phyll concentration profiles on upper-ocean radiant heating and SST requires further investigation.

The mesoscale and sub-mesoscale spatial variability of h_2 and the associated oceanic processes is inadequately represented in MC-KPP due to its coarse horizontal resolution. The coastal region in MC-KPP is represented by multiple grid points that are part ocean and part land at an approximate 90 km horizontal resolution. Such a resolution means that at the coastlines, the mesoscale coastal chlorophyll concentration features, and the corresponding solar penetration depths are poorly resolved. Future studies should consider using a high-resolution, fully dynamical model to accurately resolve the coastline and the associated solar penetration depths. The simulated dynamics would improve the representation of mesoscale eddy activity along the coast and open ocean, which increases biological productivity (Kumar et al., 2007) and, in turn, increases local solar radiation absorption.

The sub-seasonal temporal variability of h_2 is inadequately represented in MC-KPP due to the use of a monthly mean climatological chlorophyll concentration at a reduced horizontal resolution. In reality, the advection of high surface chlorophyll concentrations into the southern and central BoB varies with the strength and positioning of the SLD and SMC (Vinayachandran et al., 2004), which is itself further influenced by local wind stress and seasonal Rossby waves (Webber et al., 2018). Surface chlorophyll concentrations are periodically enhanced by transient cold-core eddies and post-monsoon cyclones in the central BoB, which briefly upwell nutrients to the ocean surface (Vinayachandran and Mathew, 2003; Patra et al., 2007). In coastal regions, nutrient concentrations, which affect surface chlorophyll concentrations, vary with river discharge (Kumar et al., 2010). Suspended terrestrial sediment that perturbs solar penetration depths on the continental shelf also depend on river discharge (Kumar et al., 2010; Lotliker et al., 2016). All of these factors influence solar penetration depths on timescales of days to weeks and on spatial scales of less than 1 km. By smoothing over the large sub-seasonal variability of the chlorophyll concentration, such variations in the solar penetration depth are not represented in the present study.

The limitations of representing ocean dynamics as a mean seasonal cycle means that MC-KPP cannot capture any ocean dynamical response to biologically induced changes in ocean properties (e.g. changes in ocean temperature and salinity transports). Previous studies have shown large effects of chlorophyll on ocean dynamics in the equatorial Pacific (e.g. Nakamoto et al., 2001; Murtugudde et al., 2002) and in mid- to high-latitude regions (e.g. Manizza et al., 2005; Patara et al., 2012). Modified biological warming at the surface or perhaps modified solar radiation penetration below the mixed layer could affect the dynamics of the SMC and SLD in the BoB. Missing modes of variability in MetUM-GOML that rely on a dynamical ocean, such as ENSO and IOD, could combine nonlinearly with the ocean anomalies induced by biological warming, with implications for monsoon rain-fall. Further research using a fully dynamical coupled ocean–atmosphere GCM is required to show the dynamical changes and feedbacks of biological warming on the BoB oceanic and atmospheric system.

Biological heating has complex physical and dynamical feedbacks in the ocean, which, in turn, imply similar feedbacks on BoB biological processes. The imposed seasonally and spatially varying h_2 in MC-KPP eliminates any biological response to secondary feedbacks in the ocean. A coupled biogeochemistry model linked to an ocean–atmosphere GCM would be needed to further understand secondary feedbacks on phytoplankton productivity. Secondary feedbacks may include changes in cloud cover that affect the incoming shortwave radiation needed for biological productivity, changes in thermal and salinity stratification that affect the vertical mixing of nutrients to the ocean surface, or changes in rainfall that affect river discharge and nutrient availability on the continental shelf which influence biological productivity. The resultant changes in biological productivity could either enhance or deplete chlorophyll concentrations at the surface, with further implications for the spatial and temporal extent of biological heating. It is important that realistic simulations of chlorophyll concentrations are included as an additional Earth system process in high-resolution coupled ocean–atmosphere GCMs, which may improve the simulated seasonality and intraseasonal variability of the South Asian monsoon.

Author contributions. JG performed the data analysis and paper preparation. NPK provided support regarding the MetUM-GOML set-up. All authors contributed to the design of the study and the data interpretation as well as giving feedback on earlier iterations of the paper.

References

Amol, P., Vinayachandran, P. N., Shankar, D., Thushara, V., Vijith, V., Chatterjee, A., and Kankonkar, A.: Effect of freshwater advection and winds on the vertical structure of chlorophyll in the northern Bay of Bengal, Deep-Sea Res. Pt. II, https://doi.org/10.1016/j.dsr2.2019.07.010, 2019.

Bernie, D. J., Woolnough, S. J., Slingo, J. M., and Guilyardi, E.: Modeling diurnal and intraseasonal variability of the ocean mixed layer, J. Climate, 18, 1190–1202, https://doi.org/10.1175/JCLI3319.1, 2005.

Bernie, D. J., Guilyardi, E., Madec, G., Slingo, J. M., Woolnough, S. J., and Cole, J.: Impact of resolving the diurnal cycle in an ocean–atmosphere GCM. Part 2: A diurnally coupled CGCM, Clim. Dynam., 31, 909–925, https://doi.org/10.1007/s00382-008-0429-z, 2008.

Blondeau-Patissier, D., Gower, J. F., Dekker, A. G., Phinn, S. R., and Brando, V. E.: A review of ocean color remote sensing methods and statistical techniques for the detection, mapping and analysis of phytoplankton blooms in coastal and open oceans, Prog. Oceanogr., 123, 123–144, https://linkinghub.elsevier.com/retrieve/pii/S0079661114000020, 2014.

Boss, E., Slade, W., and Hill, P.: Effect of particulate aggregation in aquatic environments on the beam attenuation and its utility as a proxy for particulate mass, Opt. Express, 17, 9408–9420, https://doi.org/10.1364/OE.17.009408, 2009.

Chang, G. C. and Dickey, T. D.: Coastal ocean optical influences on solar transmission and radiant heating rate, J. Geophys. Res., 109, C01020, https://https://doi.org/10.1029/2003JC001821, 2004.

Ding, Q. and Wang, B.: Circumglobal teleconnection in the Northern Hemisphere summer, J. Climate, 18, 3483–3505, https://doi.org/10.1175/JCLI3473.1, 2005.

Duncan, B. and Han, W.: Indian Ocean intraseasonal sea surface temperature variability during boreal summer: Madden-Julian Oscillation versus submonthly forcing

and processes, J. Geophys. Res.-Oceans, 114, C05002, https://doi.org/10.1029/2008JC004958, 2009.

Franz, B. A., Bailey, S. W., Werdell, P. J., and McClain, C. R.: Sensor-independent approach to the vicarious calibration of satellite ocean color radiometry, Appl. Opt., 46, 5068–5082, https://doi.org/10.1364/ao.46.005068, 2007 (data available at: https://oceancolor.gsfc.nasa.gov, last access: 9 August 2020).

Franz, B. A., Kwiatowska, E. J., Meister, G., and McClain, C. R.: Moderate Resolution Imaging Spectroradiometer on Terra: limitations for ocean color applications, J. Appl. Remote Sens., 2, 023525, https://doi.org/10.1117/1.2957964, 2008.

Giddings, J.: MetUM-GOML3.0 Chlorophyll Perturbation Datasets, figshare, https://doi.org/10.6084/m9.figshare.13084052, 2020.

Girishkumar, M. S., Ravichandran, M., McPhaden, M. J., and Rao, R. R.: Intraseasonal variability in barrier layer thickness in the south central Bay of Bengal, J. Geophys. Res.-Oceans, 116, C03009, https://doi.org/10.1029/2010JC006657, 2011.

Gnanadesikan, A. and Anderson, W. G.: Ocean water clarity and the ocean general circulation in a coupled climate model, J. Phys. Oceanogr., 39, 314–332, https://doi.org/10.1175/2008JPO3935.1, 2009.

Gomes, H. R., Goes, J. I., and Saino, T.: Influence of physical processes and freshwater discharge on the seasonality of phytoplankton regime in the Bay of Bengal, Cont. Shelf Res., 20, 313–330, https://doi.org/10.1016/S0278-4343(99)00072-2, 2000.

Hill, V. J.: Impacts of chromophoric dissolved organic material on surface ocean heating in the Chukchi Sea, J. Geophys. Res., 113, C07024, https://https://doi.org/10.1029/2007JC004119, 2008.

Hirons, L. C., Klingaman, N. P., and Woolnough, S. J.: MetUM-GOML1: a near-globally coupled atmosphere–ocean-mixed-layer model, Geosci. Model Dev., 8, 363–379, https://doi.org/10.5194/gmd-8-363-2015, 2015.

Hu, K., Huang, G., Qu, X., and Huang, R.: The impact of Indian Ocean variability on high temperature extremes across the southern Yangtze River valley in late summer, Adv. Atmos. Sci., 29, 91–100, https://doi.org/10.1007/s00376-011-0209-2, 2012a.

Hu, C., Lee, Z., and Bryan, F.: Chlorophyll *a* algorithms for oligotrophic oceans: A novel approach based on three-band reflectance difference, J. Geophys. Res.-Oceans, 117, C01011, https://doi.org/10.1029/2011JC007395, 2012b.

Hu, C., Feng, L., Lee, Z., Franz, B. A., Bailey, S. W., Werdell, P. J., and Proctor, C. W.: Improving satellite global chlorophyll *a* data products through algorithm refinement and data recovery, J. Geophys. Res.-Oceans, 124, 1524–1543, https://doi.org/10.1029/2019JC014941, 2019.

Huffman, G. J., Adler, R. F., Bolvin, D. T., Gu, G. J., Nelkin E. J., Bowman, K. P., Hoong, Y., Stocker, E. F., and Wolff, D. B.: The TRMM multisatellite precipitation analysis (TMPA): Quasi-global, multiyear, combined-sensor precipitation estimates at fine scales, J. Hydrometeorol., 8, 38–55, https://doi.org/10.1175/JHM560.1, 2007 (data available at: https://disc.gsfc.nasa.gov/datasets?keywords=precipitation, last access: 31 July 2019).

Huisman, J., Pham Thi, N. N., Karl, D. M., and Sommeijer, B.: Reduced mixing generates oscillations and chaos in the oceanic deep chlorophyll maximum, Nature, 439, 322–325, 2006.

Jana, S., Gangopadhyay, A., and Chakraborty, A.: Impact of seasonal river input on the Bay of Bengal simulation, Cont. Shelf

Res., 104, 45–62, https://doi.org/10.1016/j.csr.2015.05.001, 2015.

Jerlov, N. G.: Optical oceanography, Oceanography Series 5, Elsevier Publishing Company, Amsterdam, the Netherlands, 1968.

Ju, J. and Slingo, J.: The Asian summer monsoon and ENSO, Q. J. Roy. Meteor. Soc., 121, 1133–1168, https://doi.org/10.1002/qj.49712152509, 1995.

Kim, G. E., Gnanadesikan, A., DelCastillo, C. E., and Pradal, M.-A.: Upper ocean cooling in a coupled climate model due to light attenuation by yellowing materials, Geophys. Res. Lett., 45, 6134–6140, https://doi.org/10.1029/2018GL077297, 2018.

Klingaman, N. P., Woolnough, S. J., Weller, H., and Slingo, J. M.: The impact of finer-resolution air–sea coupling on the intraseasonal oscillation of the Indian monsoon, J. Climate, 24, 2451–2468, https://doi.org/10.1175/2010JCLI3868.1, 2011.

Kuehl, S. A., Levy, B. M., Moore, W. S., and Allison, M. A.: Subaqueous delta of the Ganges-Brahmaputra river system, Mar. Geol., 144, 81–96, https://doi.org/10.1016/S0025-3227(97)00075-3, 1997.

Kumar, S. P., Muraleedharan, P. M., Prasad, T. G., Gauns, M., Ramaiah, N., de Souza, S. N., Sardesai, S., and Madhupratap, M.: Why is the Bay of Bengal less productive during summer monsoon compared to the Arabian Sea?, Geophys. Res. Lett., 29, 2235, https://doi.org/10.1029/2002GL016013, 2002.

Kumar, S. P., Nuncio, M., Ramaiah, N., Sardesai, S., Narvekar, J., Fernandes, V., and Paul, J. T.: Eddy-mediated biological productivity in the Bay of Bengal during fall and spring intermonsoons, Deep-Sea Res. Pt. I, 54, 1619–1640, https://doi.org/10.1016/j.dsr.2007.06.002, 2007.

Kumar, S. P., Narvekar, J., Nuncio, M., Kumar, A., Ramaiah, N., Sardesai, S., Gauns, M., Fernandes, V., and Paul, J.: Is the biological productivity in the Bay of Bengal light limited?, Curr. Sci., 98, 1331–1339, 2010.

Large, W. G., McWilliams, J. C., and Doney, S. C.: Oceanic vertical mixing: A review and a model with a nonlocal boundary layer parameterization, Rev. Geophys., 32, 363, https://doi.org/10.1029/94RG01872, 1994.

Lévy, M., Shankar, D., André, J.-M., Shenoi, S. S. C., Durand, F., and de Boyer Montégut, C.: Basin-wide seasonal evolution of the Indian Ocean's phytoplankton blooms, J. Geophys. Res.-Oceans, 112, C12014, https://doi.org/10.1029/2007JC004090, 2007.

Lewis, M. R., Carr, M.-E., Feldman, G. C., Esaias, W., and McClain, C.: Influence of penetrating solar radiation on the heat budget of the equatorial Pacific Ocean, Nature, 347, 543–545, https://doi.org/10.1038/347543a0, 1990.

Li, C. and Yanai, M.: The onset and interannual variability of the Asian summer monsoon in relation to land-sea thermal contrast, J. Climate, 9, 358–375, https://doi.org/10.1175/1520-0442(1996)009<0358:TOAIVO>2.0.CO;2, 1996.

Lin, J.-L., Weickman, K. M., Kiladis, G. N., Mapes, B. E., Schubert, S. D., Suarez, M. J., Bacmeister, J. T., and Lee, M.-I.: Subseasonal variability associated with Asian summer monsoon simulated by 14 IPCC AR4 coupled GCMs, J. Climate, 21, 4541–4567, https://doi.org/10.1175/2008JCLI1816.1, 2008.

Lotliker, A. A., Omand, M. M., Lucas, A. J., Laney, S. R., Mahadevan, A., and Ravichandran, M.: Penetrative radiative flux in the Bay of Bengal, Oceanogr., 29, 214–221, https://doi.org/10.5670/oceanog.2016.53, 2016.

Manizza, M., Quéré, C. L., Watson, A. J., and Buitenhuis, E. T.: Bio-optical feedbacks among phytoplankton, upper ocean physics and sea-ice in a global model, Geophys. Res. Lett., 32, L05603, https://doi.org/10.1029/2004GL020778, 2005.

McCreary, J. P., Murtugudde, R., Vialard, J., Vinayachandran, P. N., Wiggert, J. D., Hood, R. R., Shankar, D., and Shetye, S.: Biophysical processes in the Indian Ocean, Indian Ocean biogeochemical processes and ecological variability, 185, 9–32, https://doi.org/10.1029/2008GM000768, 2009.

Meister, G. and Franz, B. A.: Corrections to the MODIS aqua calibration derived from MODIS aqua ocean color products, IEEE T. Geosci. Remote, 52, 6534–6541, https://doi.org/10.1109/TGRS.2013.2297233, 2014.

Morel, A.: Optical modeling of the upper ocean in relation to its biogenous matter content (case I waters), J. Geophys. Res.-Oceans, 93, 10749–10768, https://doi.org/10.1029/JC093iC09p10749, 1988.

Morel, A. and Antoine, D.: Heating Rate within the Upper Ocean in Relation to its Bio-optical State, J. Phys. Oceanogr., 24, 1652–1665, 1994.

Morel, A., Huot, Y., Gentili, B., Werdell, P. J., Hooker, S. B., and Franz, B. A.: Examining the consistency of products derived from various ocean color sensors in open ocean (Case 1) waters in the perspective of a multi-sensor approach, Remote Sens. Environ., 111, 69–88, https://doi.org/10.1016/j.rse.2007.03.012, 2007.

Murtugudde, R., Beauchamp, J., McClain, C. R., Lewis, M., and Busalacchi, A. J.: Effects of penetrative radiation on the upper tropical ocean circulation, J. Climate, 15, 470–486, 2002.

Nakamoto, S., Kumar, S. P., Oberhuber, J. M., Muneyama, K., and Frouin, R.: Chlorophyll modulation of sea surface temperature in the Arabian Sea in a mixed-layer isopycnal general circulation model, Geophys. Res. Lett., 27, 747–750, https://doi.org/10.1029/1999GL002371, 2000.

Nakamoto, S., Kumar, S. P., Oberhuber, J. M., Ishizaka, J., Muneyama, K., and Frouin, R.: Response of the equatorial Pacific to chlorophyll pigment in a mixed layer isopycnal ocean general circulation model, Geophys. Res. Lett., 28, 2021–2024, https://doi.org/10.1029/2000GL012494, 2001.

Narvekar, J., and Kumar, S. P.: Seasonal variability of the mixed layer in the central Bay of Bengal and associated changes in nutrients and chlorophyll. Deep-Sea Res. Pt. I, 53, 820–835, https://doi.org/10.1016/j.dsr.2006.01.012, 2006.

O'Reilly, J. E., Maritorena, S., O'brien, M. C., Siegel, D. A., Toole, D., Menzies, D., Smith, R. C., Mueller, J. L., Mitchell, B. G., Kahru, M., and Chavez, F. P.: SeaWiFS postlaunch calibration and validation analyses, part 3, NASA tech. memo., 11, 2000–206892, available at: https://oceancolor.gsfc.nasa.gov/docs/technical/seawifs_reports/postlaunch/post_vol11_abs/ (last access: 9 June 2020), 2000.

Pandi, S. R., Kiran, R., Sarma, N. S., Srikanth, A. S., Sarma, V. V. S. S., Krishna, M. S., Bandyopadhyay, D., Prasad, V. R., Acharyya, T., and Reddy, K. G.: Contrasting phytoplankton community structure and associated light absorption characteristics of the western Bay of Bengal, Ocean Dynam., 64, 89–101, https://doi.org/10.1007/s10236-013-0678-1, 2014.

Park, J.-Y. and Kug, J.-S.: Marine biological feedback associated with Indian Ocean Dipole in a coupled

ocean/biogeochemical model, Clim. Dynam., 42, 329–343, https://doi.org/10.1007/s00382-012-1640-5, 2014.

Patra, P. K., Kumar, M. D., Mahowald, N., and Sarma, V. V. S. S.: Atmospheric deposition and surface stratification as controls of contrasting chlorophyll abundance in the North Indian Ocean, J. Geophys. Res.-Oceans, 112, C05029, https://doi.org/10.1029/2006JC003885, 2007.

Patara, L., Vichi, M., Masina, S., Fogli, P. G., and Manzini, E.: Global response to solar radiation absorbed by phytoplankton in a coupled climate model, Clim. Dynam., 39, 1951–1968, https://doi.org/10.1007/s00382-012-1300-9, 2012.

Paulson, C. A. and Simpson, J. J.: Irradiance measurements in the upper ocean, J. Phys. Oceanogr., 7, 952–956, 1977.

Peatman, S. C. and Klingaman, N. P.: The Indian summer monsoon in MetUM-GOML2.0: effects of air–sea coupling and resolution, Geosci. Model Dev., 11, 4693–4709, https://doi.org/10.5194/gmd-11-4693-2018, 2018.

Pramanik, S., Sil, S., Gangopadhyay, A., Singh, M. K., and Behera, N.: Interannual variability of the chlorophyll-a concentration over Sri Lankan Dome in the Bay of Bengal, Int. J. Remote Sens., 41, 1–18, https://doi.org/10.1080/01431161.2020.1727057, 2020.

Rao, R. R. and Sivakumar, R.: Seasonal variability of sea surface salinity and salt budget of the mixed layer of the north Indian Ocean, J. Geophys. Res.-Oceans, 108, 3009, https://doi.org/10.1029/2001JC000907, 2003.

Sengupta, D., Bharath Raj, G. N., Ravichandran, M., Sree Lekha, J., and Papa, F.: Near-surface salinity and stratification in the north Bay of Bengal from moored observations, Geophys. Res. Lett., 43, 4448–4456, https://doi.org/10.1002/2016GL068339, 2016.

Shee, A., Sil, S., Gangopadhyay, A., Gawarkiewicz, G., and Ravichandran, M.: Seasonal evolution of oceanic upper layer processes in the northern Bay of Bengal following a single Argo float, Geophys. Res. Lett., 46, 5369–5377, https://doi.org/10.1029/2019GL082078, 2019.

Shell, K. M., Frouin, R., Nakamoto, S., and Somerville, R. C. J.: Atmospheric response to solar radiation absorbed by phytoplankton, J. Geophys. Res.-Atmos., 108, 4445, https://doi.org/10.1029/2003JD003440, 2003.

Shenoi, S. S. C., Shankar, D., and Shetye, S. R.: Differences in heat budgets of the near-surface Arabian Sea and Bay of Bengal: Implications for the summer monsoon, J. Geophys. Res.-Oceans, 107, 3052, https://doi.org/10.1029/2000JC000679, 2002.

Smith, D. M. and Murphy, J. M.: An objective ocean temperature and salinity analysis using covariances from a global climate model, J. Geophys Res.-Oceans, 112, C02022, https://doi.org/10.1029/2005JC003172, 2007.

Sperber, K. R., Annamalai, H., Kang, I.-S., Kitoh, A., Moise, A., Turner, A., Wang, B., and Zhou, T.: The Asian summer monsoon: an intercomparison of CMIP5 vs. CMIP3 simulations of the late 20th century, Clim. Dynam., 41, 2711–2744, https://doi.org/10.1007/s00382-012-1607-6, 2013.

Sprintall, J. and Tomczak, M.: Evidence of the barrier layer in the surface layer of the tropics, J. Geophys. Res.-Oceans, 97, 7305–7316, https://doi.org/10.1029/92JC00407, 1992.

Stephan, C. C., Klingaman, N. P., and Turner, A. G.: A mechanism for the recently increased interdecadal variability of the silk road pattern, J. Climate, 32, 717–736, https://doi.org/10.1175/JCLI-D-18-0405.1, 2019.

Thompson, V., Dunstone, N. J., Scaife, A. A., Smith, D. M., Hardiman, S. C., Ren, H. L., Lu, B., and Belcher, S. E.: Risk and dynamics of unprecedented hot months in South East China, Clim. Dynam., 52, 2585–2596, https://doi.org/10.1007/s00382-018-4281-5, 2019.

Thushara, V., Vinayachandran, P. N. M., Matthews, A. J., Webber, B. G. M., and Queste, B. Y.: Vertical distribution of chlorophyll in dynamically distinct regions of the southern Bay of Bengal, Biogeosciences, 16, 1447–1468, https://doi.org/10.5194/bg-16-1447-2019, 2019.

Tilstone, G. H., Angel-Benavides, I. M., Pradhan, Y., Shutler, J. D., Groom, S., and Sathyendranath, S.: An assessment of chlorophyll-a algorithms available for SeaWiFS in coastal and open areas of the Bay of Bengal and Arabian Sea, Remote Sens. Environ., 115, 2277–2291, https://doi.org/10.1016/j.rse.2011.04.028, 2011.

Tilstone, G. H., Lotliker, A. A., Miller, P. I., Ashraf, P. M., Kumar, T. S., Suresh, T., Ragavan, B. R., and Menon, H. B.: Assessment of MODIS-Aqua chlorophyll-a algorithms in coastal and shelf waters of the eastern Arabian Sea, Cont. Shelf Res., 65, 14–26, https://doi.org/10.1016/j.csr.2013.06.003, 2013.

Turner, A. G., Joshi, M., Robertson, E. S., and Woolnough, S. J.: The effect of Arabian Sea optical properties on SST biases and the South Asian summer monsoon in a coupled GCM, Clim. Dynam., 39, 811–826, https://doi.org/10.1007/s00382-011-1254-3, 2012.

Valcke, S.: The OASIS3 coupler: a European climate modelling community software, Geosci. Model Dev., 6, 373–388, https://doi.org/10.5194/gmd-6-373-2013, 2013.

Vecchi, G. A. and Harrison, D. E.: Monsoon breaks and subseasonal sea surface temperature variability in the Bay of Bengal, J. Climate, 15, 1485–1493, 2002.

Vinayachandran, P. N. and Yamagata, T.: Monsoon response of the sea around Sri Lanka: generation of thermal domes and anticyclonic vortices, J. Phys. Oceanogr., 28, 1946–1960, 1998.

Vinayachandran, P. N., Murty, V. S. N., and Ramesh Babu, V.: Observations of barrier layer formation in the Bay of Bengal during summer monsoon, J. Geophys. Res.-Oceans, 107, 8018, https://doi.org/10.1029/2001JC000831, 2002.

Vinayachandran, P. N. and Mathew, S.: Phytoplankton bloom in the Bay of Bengal during the northeast monsoon and its intensification by cyclones, Geophys. Res. Lett., 30, 1572, https://doi.org/10.1029/2002GL016717, 2003.

Vinayachandran, P. N., Chauhan, P., Mohan, M., and Nayak, S.: Biological response of the sea around Sri Lanka to summer monsoon, Geophys. Res. Lett., 31, L01302, https://doi.org/10.1029/2003GL018533, 2004.

Walters, D., Baran, A. J., Boutle, I., Brooks, M., Earnshaw, P., Edwards, J., Furtado, K., Hill, P., Lock, A., Manners, J., Morcrette, C., Mulcahy, J., Sanchez, C., Smith, C., Stratton, R., Tennant, W., Tomassini, L., Van Weverberg, K., Vosper, S., Willett, M., Browse, J., Bushell, A., Carslaw, K., Dalvi, M., Essery, R., Gedney, N., Hardiman, S., Johnson, B., Johnson, C., Jones, A., Jones, C., Mann, G., Milton, S., Rumbold, H., Sellar, A., Ujiie, M., Whitall, M., Williams, K., and Zerroukat, M.: The Met Office Unified Model Global Atmosphere 7.0/7.1 and JULES Global Land 7.0 configurations, Geosci. Model Dev., 12, 1909–1963, https://doi.org/10.5194/gmd-12-1909-2019, 2019.

Wang, M., Knobelspiesse, K. D., and McClain, C. R.: Study of the Sea-Viewing Wide Field-of-View Sensor (SeaWiFS) aerosol optical property data over ocean in combination with the ocean color products, J. Geophys. Res.-Atmos., 110, D10S06, https://doi.org/10.1029/2004JD004950, 2005.

Wang, M. and Son, S.: VIIRS-derived chlorophyll-*a* using the ocean color index method, Remote Sens. Environ., 182, 141–149, https://doi.org/10.1016/j.rse.2016.05.001, 2016.

Webber, B. G. M., Matthews, A. J., Vinayachandran, P. N., Neema, C. P., Sanchez-Franks, A., Vijith, V., Amol, P., and Baranowski, D. B.: The dynamics of the Southwest Monsoon current in 2016 from high-resolution in situ observations and model, J. Phys. Oceanogr., 48, 2259–2282, https://doi.org/10.1175/JPO-D-17-0215.1, 2018.

Webster, P. J., Magaña, V. O., Palmer, T. N., Shukla, J., Tomas, R. A., Yanai, M., and Yasunari, T.: Monsoons: Processes, predictability, and the prospects for prediction, J. Geophys. Res.-Ocean, 103, 14451–14510, https://doi.org/10.1029/97JC02719, 1998.

Wetzel, P., Maier-Reimer, E., Botzet, M., Jungclaus, J., Keenlyside, N., and Latif, M.: Effects of ocean biology on the penetrative radiation in a coupled climate model, J. Climate, 19, 3973–3987, https://doi.org/10.1175/JCLI3828.1, 2006.

Zaneveld, J. R. V., Kitchen, J. C., and Pak, H.: The influence of optical water type on the heating rate of a constant depth mixed layer, J. Geophys. Res.-Oceans, 86, 6426–6428, https://doi.org/10.1029/JC086iC07p06426, 1981.